Multivariate morphometry statistics reveal the morphological change pattern of hippocampus during normal aging

Hong Chai[a], Jianhua Sun[b], Peng Zhou[a] and Lingyu Zhang[c]; for the Alzheimer's Disease Neuroimaging Initiative (ADNI)*

There have been numerous studies focusing on normal aging in previous decades which is accompanied by the structural and functional decline in the hippocampus, while the pattern of hippocampal alteration with age remains unclear. Figuring out the mechanism of hippocampal changes precisely is beneficial for a better understanding of the aging process. In this study, we included a total of 451 T1 MRI scans of subjects of age 50–90 who were labeled as normal in the Alzheimer's Disease Neuroimaging Initiative. Taking 10 years of age as an age band, we divided the subjects into four groups (denoted as HC1, HC2, HC3, and HC4, respectively), with the youngest being 50–60 and the oldest 81–90. Then the Multivariate Morphometry Statistics (MMS) of the hippocampus segmented from the four groups were extracted by surface reconstruction, mesh generation, and surface registration. Finally, the significant differences between the youngest group and the other three were statistically analyzed. Results showed that the earliest deformation region of the left hippocampus located in the frontal subiculum and the dorsal CA1 of the tail part and gradually expanded with aging, while the right hippocampal deformation mainly concentrated in the dorsal CA1 and spread to the posterior CA2-3, which occurred later than that of the left. All the results illustrated that the hippocampus is truly a vulnerable structure in the course of aging, and the MMS are sensitive metrics for detecting the changes in the subcortical convex structure.

NeuroReport 2022, **33**:481–486

Keywords: aging, hippocampus, MRI, surface-based morphometry

[a]Department of Computer Science and Technology, School of Electronic and Information Engineering, Lanzhou Jiaotong University, [b]Gansu Keyuan Power Group Tongxing Zhineng Technology Development Corporation and [c]Department of Computer Science and Technology, Gansu Provincial Key Laboratory of Wearable Computing, School of Information Science and Engineering, Lanzhou University, Lanzhou, China

Correspondence to Lingyu Zhang, Department of Computer Science and Technology, School of Information Science and Engineering, Lanzhou University, Lanzhou 730000, China
Tel: +86 13038707361; e-mail: lyzhang21@lzu.edu.cn

*Data used in preparation of this article were obtained from the Alzheimer's Disease Neuroimaging Initiative (ADNI) database (adni.loni.usc.edu). As such, the investigators within the ADNI contributed to the design and implementation of ADNI and/or provided data but did not participate in analysis or writing of this report. A complete listing of ADNI investigators can be found at: http://adni.loni.usc.edu/wp-content/uploads/how_to_apply/ADNI_Acknowledgement_List.pdf

Received 18 May 2022 **Accepted** 31 May 2022

Introduction

Increasing age is expected to raise the high risk of age-related diseases such as Alzheimer's disease, and elderly individuals are susceptible to suffer cognitive decline. During the process of aging, the hippocampus has undergone drastic changes [1], and its lesions have been widely considered the defining pathology of cognitive decline [2]. Actually, the aging process is characterized by complexity and heterogeneity and involves a wide range of neuropathological bases. Although there is already a multitude of studies that have investigated the role of the hippocampus in aging, most of which focused on the conventional indicators such as the volume or area of the whole hippocampus [3], which are not sensitive enough to the subcortical nuclei so that it is difficult to detect the subtle local deformation. Therefore, the precise mechanism of the morphological alteration pattern is still unknown.

Some scholars have investigated the hippocampal changes in the aging process using voxel-based morphometry (VBM), which is more detailed and can detect local abnormality of the gray matter in the case of accurate registration to a certain extent, and resulted in promising results [4]. However, due to the existence of the artifacts, the positive results often need to be verified again. Previous studies have demonstrated that surface-based morphometry (SBM) exhibits a powerful ability to probe the alteration associated with advancing aging [5], but just like the VBM method mentioned above, it also relies on accurate registration. To solve this problem, a novel registration framework was introduced in this study, which can obtain accurate registration without the need for precise surface normal.

In this article, three SBM indicators, including the radial distance (RD), surface tensor-based morphometry (TBM), and the surface multi-variate TBM (mTBM), were extracted from 451 T1 MRI scans of healthy elderly by surface conformal parameterization, conformal presentation, and fluid registration. RD and mTBM were combined into a vector called multivariate morphometry

DOI: 10.1097/WNR.0000000000001810

statistics (MMS) given the confirmed potent statistical performance in our previous work [6]. All of these indicators were analyzed statistically to identify the areas with significant differences between the youngest group and the older ones. After calculation, we depicted the precise hippocampal alteration pattern of atrophy or expansion of the 15 000 surface vertices during the aging process. A brief workflow of this study is illustrated in Fig. 1.

Methods

Participants

All the 451 T1 MRI scans used in this study were obtained from the Alzheimer's Disease Neuroimaging Initiative (ADNI) database (https://adni.loni.usc.edu/) launched in 2003, which was led by Principal Investigator Michael W. Weiner, MD with testing whether serial MRI, PET, other biological markers, and clinical assessment can be combined to quantify the progression of Alzheimer's disease. In this study, the criteria for the normal older adults included Mini-mental State Examination score within the range 24–30, a clinical dementia rating score of 0 with the Memory Box score being 0, and age greater than 50. Taking 10 years of age as an age band, we divided the subjects into four groups HC1 (24 subjects of age 50–60), HC2 (187 subjects of age 61–70), HC3 (179 subjects of age 71–80), and HC4 (61 subjects of age 81–90). Detailed demographical and clinical information of subjects are summarized in Table 1.

Data processing and feature extraction

First, the hippocampus was defined anatomically using FSLs subcortical segmentation protocol (FIRST). Second, the surface models were built using the topology-preserving level set method [7], on which the triangular surface meshes were constructed using the marching cube algorithm [8], as shown in Fig. 1(d). Surfaces that failed to model were removed during a strict manual visual inspection step. For more suitable surfaces to generate the conformal grids, the surfaces were smoothed, which included mesh simplification [9] and mesh refinement [10] following our previous studies [11]. Then, the conformal grids were computed with the holomorphic 1-form basis on the Euclidean domain [12], based on which the surface geometric features were obtained using surface conformal representation. Finally, a fluid registration method [13] was used to register surfaces to a common template to obtain 15 000 indexed vertices on each surface, so that we obtained the one-to-one correspondence between the single surface and template, which allows us to analyze the morphological changes

Fig. 1

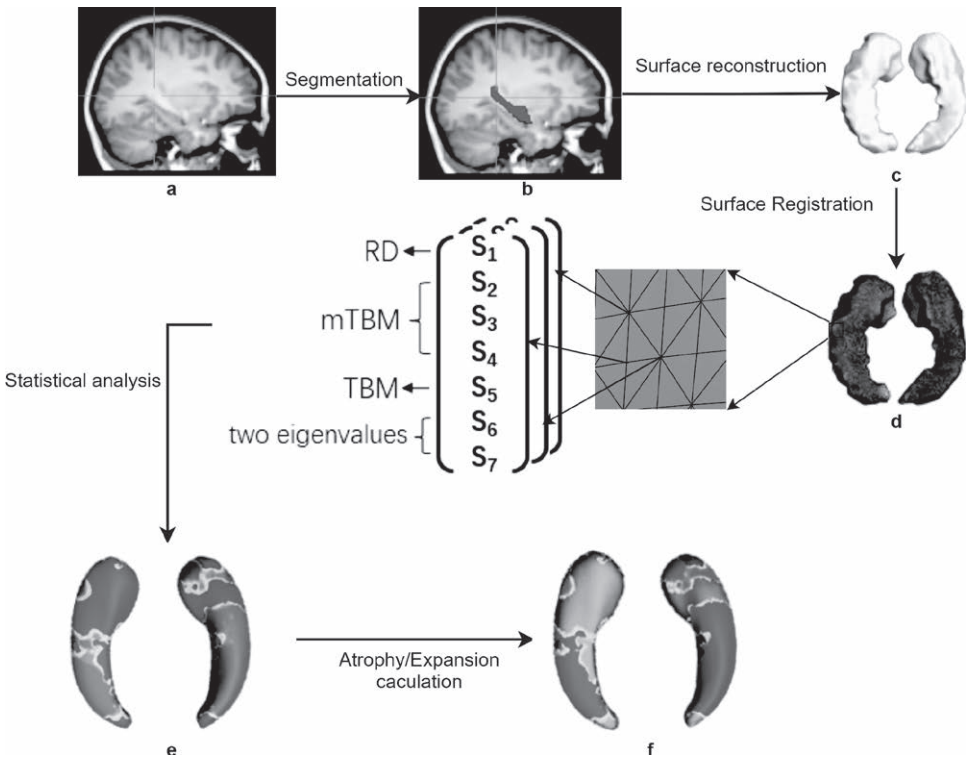

The overall workflow developed in this study. (a) T1 MRI; (b) hippocampus segmented from (a); (c) the constructed 3D surface; (d) the generated meshes representing the one-to-one correspondence; (e) areas with significant differences; (f) areas with atrophy or expansion. mTBM, the surface multivariate TBM; RD, radial distance; TBM, determinant of the Jacobian matrix.

Table 1 Demographic information of subjects

					p value		
Variables	HC1	HC2	HC3	HC4	HC1 vs. HC2	HC1 vs. HC3	HC1 vs. HC4
Sample size	24	187	179	61	–	–	–
Age (means±SD)	57.88±1.650	66.87±2.372	74.55±2.783	83.80±2.337	–	–	–
Sex (male/female)	8/16	57/130	70/109	36/25	0.816[a]	0.66[a]	0.053[a]
MMSE (means±SD)	29.42±0.717	29.16±1.055	29.01±1.173	28.93±1.365	0.25[b]	0.096[b]	0.105[b]
CDR (Memory Box)	0 (0)	0 (0)	0 (0)	0 (0)	–	–	–

HC1, subjects of age 50–60; HC2, subjects of age 61–70; HC3, subjects of age 71–80; HC4, subjects of age 81–90.
CDR, the clinical dementia rating score; MMSE, Mini-mental State Examination score.
[a]Chi-square test.
[b]Two-sample *T* test.

precisely. The detailed introduction of the conformal representation was as follows: conformal mapping is also called conformal mapping. Conformal mapping at a point means that the angle and direction of the intersection curve after mapping remain at this point. Here, conformal mapping keeps the inner angle of the triangular patch of the reconstructed hippocampal surface unchanged before and after mapping.

Given S be a surface inR^3, and $\{(U_\alpha,z_\alpha)\}$ is the atlas of S, where U_α refers to the open set of S and z_α is the mapping from the open set U_α to the complex plane C. The differential 1-form of the local parameter (x_α,y_α) on the coordinate chart (U_α,z_α) which introduces conformal parameters between the surface patch and the image plane is defined as follows:

$$\omega = f(x_\alpha, y_\alpha)dx_\alpha + g(x_\alpha, y_\alpha)dy_\alpha \tag{1}$$

where f and g are smooth functions, and the conjugate differential 1-form is formulated as [14]:

$$^*\omega = -g(x_\alpha, y_\alpha)dx_\alpha + f(x_\alpha, y_\alpha)dy_\alpha \tag{2}$$

Then, the holomorphic 1-form is as follows:

$$\tau = \omega + \sqrt{-1}^*\omega \tag{3}$$

And the conformal parameterization ϕ of the point p on the surface S is defined as:

$$\phi(p) = \int_\gamma \tau \tag{4}$$

where γ is an arbitrary path of p to a fixed point on the surface. Apparently,ϕ is a function from S to the Euclidean planeR^2.

It can be easily proved by Gauss and Codazzi equation that the only surface S in R^3can be determined by the conformal factor and average curvature. Therefore, it is called 'conformal representation of surface', in which the conformal factor of a vertex p is:

$$\lambda(p) = \frac{\text{Area}\ [\ B_\varepsilon(p)\ ]}{\text{Area}\ \{\ \phi\ [\ B_\varepsilon(p)\ ]\ \}}\# \tag{5}$$

where $B_\varepsilon(p)$ is an open ball with p as center and ε as radius, based on which the average curvature is defined as:

$$H = \frac{1}{2\lambda}\text{sign}(\phi)\,|\triangle\,\phi| \tag{6}$$

where $\text{sign}(\phi) = \frac{<\triangle\phi,\vec{N}>}{|\triangle\phi|}$, and $\vec{N}$ is the surface normal. That is, the surface normal is only needed to calculate $\text{sign}(\phi)$ with a value of –11 or 1, so that accurate mean curvature can be achieved even when the surface normal are imprecise.

Statistical analysis

The features adopted in this study include RD (the radial distance from a vertex to the central axis), TBM (reflects the tangential alteration) [15], mTBM (3×1 vector, the supplement and reinforcement of TBM) [16] and MMS (4×1 vector, combined with RD and mTBM, which has been demonstrated powerful ability to probe the alteration) [17].

To determine the areas with significant differences between HC1 and the other three groups, the *t* test was used to analyze RD and TBM and the Hotelling's T^2 test was used for mTBM and MMS. And a vertex-based permutation test and a whole hippocampus-based permutation test were performed for multiple comparisons [6].

T value was calculated on each vertex of each surface of the two groups to represent the difference between groups based on real labels, then the surfaces of the two groups were mixed and randomly divided into two groups, and the *t* value was recalculated as *t′*. At each vertex, the ratio of *t′* value greater than *t* value to the total permutation number (10000) was taken as the *p* value, and $p = 0.05$ was taken as the threshold to establish the surface significance *p*-map (uncorrected).

The feature of the p-map was defined as the number of p values less than the threshold (0.05), which was used as the real effect. Then the features of the real and random groups are compared and the ratio of the features of the latter greater than or equal to the real effect is the probability that the observed real effect is 'accidental', so that the ratio was considered to be the global significance of the whole surface after multiple comparison correction (corrected for multiple comparisons).

Then we compared the mean RD and TBM at every vertex with p value less than 0.05 of HC2, HC3, and HC4 with HC1, respectively, as follows, to determine whether the tissue at this vertex has atrophied or expanded:

$$\begin{cases} \frac{1}{n_1}\sum_{i=1}^{n_1} X_1^i - \frac{1}{n_2}\sum_{i=1}^{n_2} X_2^i > 0 & p < 0.05: \text{ atrophy} \\ \frac{1}{n_1}\sum_{i=1}^{n_1} X_1^i - \frac{1}{n_2}\sum_{i=1}^{n_2} X_2^i < 0 & p < 0.05: \text{ expasion} \end{cases}$$

where n_1 and n_2 represent the subjects number of HC1 and another group compared (HC2, HC3, or HC4) and X_1 and X_2 represent the value of RD or TBM of HC1 and the compared group (same as above).

Results

As shown in the p-map of RD depicted in Fig. 2, the area of the earliest radial deformation of the left hippocampus was located in the frontal subiculum and posterior CA1 of the tail part and both the significance and area increased gradually, while the tangential changes surrounded the tail then spread to head with age. As for the right hippocampus, the radial deformation was distributed in dorsal CA1 and ventral CA2-3, and eventually spread to a small area of ventral subiculum, while the tangential deformation was concentrated in dorsal CA1 of the tail according to the p-map of TBM and mTBM.

After calculation, it was determined that the radial deformation of both the left and right hippocampus was atrophy. And the tail of the left hippocampus and the whole right hippocampus showed atrophy too, while the dorsal CA1 on the head of the left hippocampus expanded, as shown in Fig. 3.

When comparing HC1 with HC2, only the p values of RD and TBM in the left hippocampus reached a significant level, and the p values of mTBM, MMS, and all statistics of the right hippocampus were greater than 0.05. In comparison with HC1 and HC3, the p values of all statistics of the left hippocampus were less than 0.05, and only p value of RD of the right hippocampus reached a significant level. When the ages of the experimental group were over 81, the p values of all the indexes of the left and right hippocampus were far less than 0.05.

Discussion

Although we enrolled the elderly with normal cognition, there were significant changes in the hippocampus of the elderly, which were mainly concentrated in dorsal CA1 and the subiculum, in their 60s, 70s, and 80s compared with those in their 50s. As one of the regions most affected by the age-related disease, the CA1 subregion of the hippocampus is widely believed to be highly correlated with cognitive process, and the deformation of which may lead to the decline of working memory, spatial memory, and decision-making functions [18]. And there has been evidence of the relevance of the subiculum to memory retrieval and verbal memory [19], which might be another potential neuropathological basis for related memory deficits in the elderly. As for the direction of deformation, as shown in Fig. 3, the radial deformation of both the left and right hippocampus was atrophy, the tail of the left hippocampus and the whole right hippocampus showed atrophy too, and only the dorsal CA1 on the head of the left hippocampus expanded, which is consistent with what most classic studies have reported [20], and from a neuropathological point of view, it is associated with neuron loss and tangles [21].

In line with the previous study, these areas are not the same as the deformed areas caused by Mild Cognitive Impairment (MCI) or Alzheimer's disease [22,23], indicating that the process of normal aging is different from the pathological pathway of MCI or Alzheimer's disease, which is why MCI or Alzheimer's disease cannot be simply understood as the accelerated normal aging process. This conclusion also demonstrated one of the advantages of the method we introduced, that is, the refined features we extracted can probe the local changes. Even though some global p values are NS in Table 2, the p values after permutation test on some vertices reached a significant level, and these subtle changes cannot be detected by a method based on the overall volume of the hippocampus.

In addition, the left-right asymmetry attracted attention. Specifically, the p values of the left hippocampus were lower than that of the right one in all three comparisons. Especially in the comparison of HC1 and HC2 groups, the p values of RD and TBM in the left hippocampus reached a significant level while the global significance of all the four indicators of the right hippocampus was greater than the threshold of 0.05. It can be seen from Table 2 that the p values of the left hippocampus were all one order of magnitude larger than that of the right hippocampus. Combined with Fig. 2, the area of inter-group significance region of the left hippocampus was also larger, that is, the deformation of the left one occurred earlier and the affected area is larger than the right hippocampus, which has been suggested that this may partly be due to the deformation of the right one is mainly internal [18], while one view is that the left-right asymmetry

Fig. 2

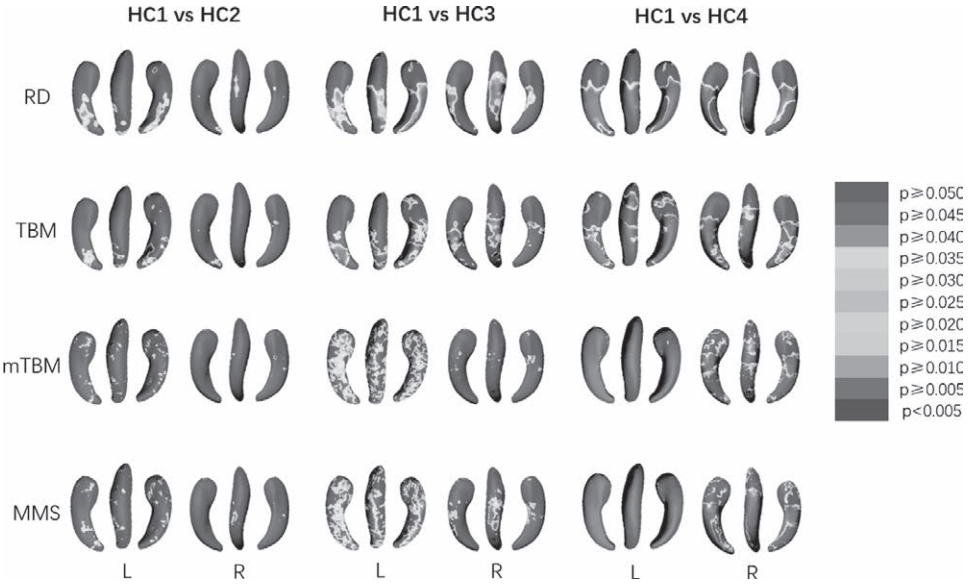

The *p*-map of surfaces.

Fig. 3

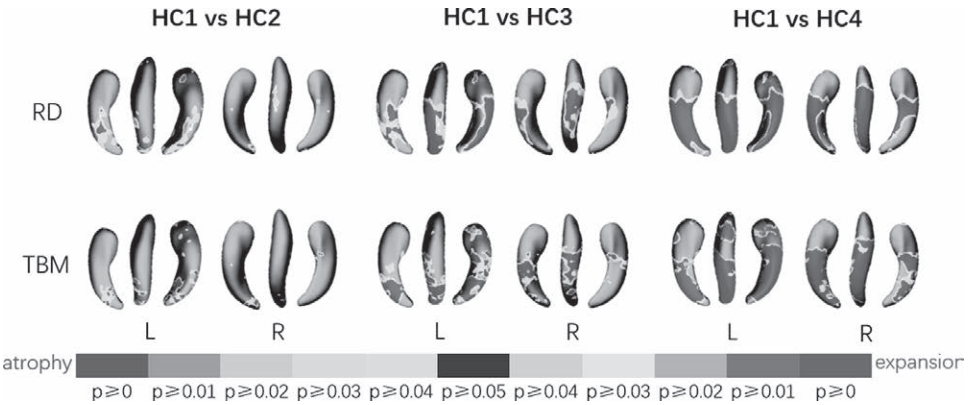

Areas with atrophy and expansion.

Table 2 **The global *p* values of HC1 and HC2, HC1 and HC3, as well as HC1 and HC4**

	HC1 vs. HC2		HC1 vs. HC3		HC1 vs. HC4	
	L	R	L	R	L	R
TBM	**0.0299**	0.2609	**0.0043**	0.052	**<0.0001**	**0.0001**
RD	**0.0254**	0.223	**0.0012**	**0.0466**	**<0.0001**	**0.0012**
mTBM	0.0893	0.6521	**0.0094**	0.216	**<0.0001**	**0.0154**
MMS	0.0906	0.5498	**0.0039**	0.0912	**<0.0001**	**0.0043**

L, the left hippocampus; R, the right hippocampus; *p* values in bold, statistical results less than 0.05.
mTBM, the surface multivariate TBM; MMS, Multivariate Morphometry Statistics; RD, radial distance; TBM, determinant of the Jacobian matrix.

underlies the human cognitive by facilitates the formation of specialized modules in the brain [24,25].

There remain some additional limitations. First, due to the consideration of preciseness, the clinical scores of subjects were strictly required, which resulted in the relatively small number of HC1 group. Second, our algorithm only aims at the subcortical convex structures, and how to apply its idea to the cortex remains to be further studied. Finally, whether there is a causal relationship between these sub-regions is also the focus of our future research.

Acknowledgements

This work was supported by the Natural Science Foundation of Gansu Province of China (Grant No. 21JR7RA286).

Data collection and sharing for this project were funded by the Alzheimer's Disease Neuroimaging Initiative (ADNI) (National Institutes of Health Grant U01 AG024904) and DOD ADNI (Department of Defense award number W81XWH-12-2-0012). ADNI is funded by the National Institute on Aging, the National Institute of Biomedical Imaging and Bioengineering, and through generous contributions from the following: AbbVie, Alzheimer's Association; Alzheimer's Drug Discovery Foundation; Araclon Biotech; BioClinica, Inc.; Biogen; Bristol-Myers Squibb Company; CereSpir, Inc.; Cogstate; Eisai Inc.; Elan Pharmaceuticals, Inc.; Eli Lilly and Company; EuroImmun; F. Hoffmann-La Roche Ltd. and its affiliated company Genentech, Inc.; Fujirebio; GE Healthcare; IXICO Ltd.; Janssen Alzheimer Immunotherapy Research & Development, LLC.; Johnson & Johnson Pharmaceutical Research & Development LLC.; Lumosity; Lundbeck; Merck & Co., Inc.; Meso Scale Diagnostics, LLC.; NeuroRx Research; Neurotrack Technologies; Novartis Pharmaceuticals Corporation; Pfizer Inc.; Piramal Imaging; Servier; Takeda Pharmaceutical Company; and Transition Therapeutics. The Canadian Institutes of Health Research is providing funds to support ADNI clinical sites in Canada. Private sector contributions are facilitated by the Foundation for the National Institutes of Health (www.fnih.org). The grantee organization is the Northern California Institute for Research and Education, and the study is coordinated by the Alzheimer's Therapeutic Research Institute at the University of Southern California. ADNI data are disseminated by the Laboratory for Neuro Imaging at the University of Southern California.

Conflicts of interest

There are no conflicts of interest.

References

1 Sele S, Liem F, Mérillat S, Jäncke L. Decline variability of cortical and subcortical regions in aging: A Longitudinal Study. *Front Hum Neurosci* 2020; **14**:363.
2 Tian J, Duo L, Sui S, Driskill C, Phensy A, Wang Q, *et al*. Disrupted hippocampal growth hormone secretagogue receptor 1α interaction with dopamine receptor D1 plays a role in Alzheimer's disease. *Sci Transl Med* 2019; **11**:eaav6278.
3 Driscoll I, Hamilton DA, Petropoulos H, Yeo RA, Brooks WM, Baumgartner RN, Sutherland RJ. The aging hippocampus: cognitive, biochemical and structural findings. *Cereb Cortex* 2003; **13**:1344–1351.
4 Woodworth DC, Scambray KA, Phelan MP, Corrada MMM, Kawas CH, Sajjadi SA. Distinct patterns of gray matter atrophy in hippocampal sclerosis of aging and Alzheimer's disease. Neuropathology. *Alzheimers Dement* 2020; **16**:e046089.
5 Wang G, Zhou W, Kong D, Qu Z, Ba M, Hao J, *et al*; Alzheimer's Disease Neuroimaging Initiative. Studying APOE ε4 allele dose effects with a univariate morphometry biomarker. *J Alzheimers Dis* 2022; **85**:1233–1250.
6 Yao Z, Fu Y, Wu J, Zhang W, Yu Y, Zhang Z, *et al*. Morphological changes in subregions of hippocampus and amygdala in major depressive disorder patients. *Brain Imaging Behav* 2020; **14**:653–667.
7 Han X, Xu C, Prince JL. A topology preserving level set method for geometric deformable models. *IEEE Trans Pattern Anal Mach Intell* 2015; **25**:755-768.
8 Lorensen WE, Cline HE. Marching cubes: a high resolution 3D surface construction algorithm. *SIGGRAPH Comput Graph* 1987; **21**:163–169.
9 Hoppe H. Progressive meshes. In: Proceedings of the 23rd Annual Conference on Computer Graphics and Interactive Techniques, New Orleans, LA, USA. August 4-9, 1996. pp. 99–108.
10 Loop CT. Smooth subdivision surfaces based on triangles. 1987. https://www.microsoft.com/en-us/research/wp-content/uploads/2016/02/thesis-10.pdf. Accessed 9 June 2022.
11 Fu Y, Zhang J, Li Y, Shi J, Zou Y, Guo H, *et al*. A novel pipeline leveraging surface-based features of small subcortical structures to classify individuals with autism spectrum disorder. *Prog Neuropsychopharmacol Biol Psychiatry* 2021; **104**:109989.
12 Wang Y, Lui LM, Gu X, Hayashi KM, Chan TF, Toga AW, *et al*. Brain surface conformal parameterization using Riemann surface structure. *IEEE Trans Med Imaging* 2007; **26**:853–865.
13 Leow A, Huang SC, Geng A, Becker J, Davis S, Toga A, Thompson P. Inverse consistent mapping in 3D deformable image registration: its construction and statistical properties. *Inf Process Med Imaging* 2005; **19**:493–503.
14 Shi J, Wang Y, Thompson PM, Wang Y. Hippocampal Morphometry Study by automated surface fluid registration and its application to Alzheimer's disease. In: Proceedings of the Third International Workshop on Mathematical Foundations of Computational Anatomy-Geometrical and Statistical Methods for Modelling Biological Shape Variability in Toronto. September 22, 2011. pp. 170-181.
15 Chung MK, Dalton KM, Davidson RJ. Tensor-based cortical surface morphometry via weighted spherical harmonic representation. *IEEE Trans Med Imaging* 2008; **27**:1143–1151.
16 Wang Y, Yuan L, Shi J, Greve A, Ye J, Toga AW, *et al*. Applying tensor-based morphometry to parametric surfaces can improve MRI-based disease diagnosis. *Neuroimage* 2013; **74**:209–230.
17 Zhang J, Stonnington C, Li Q, Shi J, Bauer RJ 3rd, Gutman BA, *et al*. Applying sparse coding to surface multivariate tensor-based morphometry to predict future cognitive declinE. *Proc IEEE Int Symp Biomed Imaging* 2016; **2016**:646–650.
18 Chandrasekaran K, Choi J, Arvas MI, Salimian M, Singh S, Xu S, *et al*. Nicotinamide mononucleotide administration prevents experimental diabetes-induced cognitive impairment and loss of hippocampal neurons. *Int J Mol Sci* 2020; **21**:E3756.
19 Eldridge LL, Engel SA, Zeineh MM, Bookheimer SY, Knowlton BJ. A dissociation of encoding and retrieval processes in the human hippocampus. *J Neurosci* 2005; **25**:3280–3286.
20 Sele S, Liem F, Mérillat S, Jäncke L. Age-related decline in the brain: a longitudinal study on inter-individual variability of cortical thickness, area, volume, and cognition. *Neuroimage* 2021; **240**:118370.
21 Hyman BT, Van Hoesen GW, Damasio AR, Barnes CL. Alzheimer's disease: cell-specific pathology isolates the hippocampal formation. *Science* 1984; **225**:1168–1170.
22 Lee P, Ryoo H, Park J, Jeong Y; Alzheimer's Disease Neuroimaging Initiative. Morphological and microstructural changes of the hippocampus in early MCI: a study utilizing the Alzheimer's Disease Neuroimaging Initiative database. *J Clin Neurol* 2017; **13**:144–154.
23 Apostolova LG, Dinov ID, Dutton RA, Hayashi KM, Toga AW, Cummings JL, Thompson PM. 3D comparison of hippocampal atrophy in amnestic mild cognitive impairment and Alzheimer's disease. *Brain* 2006; **129**:2867–2873.
24 Postema MC, van Rooij D, Anagnostou E, Arango C, Auzias G, Behrmann M, *et al*. Altered structural brain asymmetry in autism spectrum disorder in a study of 54 datasets. *Nat Commun* 2019; **10**:4958.
25 Deep-Soboslay A, Hyde TM, Callicott JP, Lener MS, Verchinski BA, Apud JA, *et al*. Handedness, heritability, neurocognition and brain asymmetry in schizophrenia. *Brain* 2010; **133**:3113–3122.